CHAPTER 5 - MODEL AND METHODOLOGY FOR CRACK DETECTION ON A FLUID-FILLED CYLINDRICAL HOLE

5.1 Background

The weep hole inspection procedure presented in Chapter 3 requires that the fuel compartments in the wing be completely purged of fuel before inspection can begin. Emptying and purging fuel from the wing during depot maintenance of the aircraft is part of the current maintenance procedure. However, due to the time and cost of emptying and drying out a wing, the capability of weep hole inspection with a wing containing fuel at locations beyond depot maintenance is of interest to the Air Force.

A review of work examining the ultrasonic scattering of waves at the cylindrical interface between elastic and fluid media was performed by Hassan and Nagy [18]. Solomon et al. formulated the scattering of elastic waves from a cylindrical fluid-filled hole by a plane shear wave. However, their analysis did not clearly demonstrate the elastic wave phenomena needed for ultrasonic inspection [50]. Hassan and Nagy have investigated the effect of the presence of a fluid on the performance of the two-element weep hole inspection technique for top cracks [18-21]. First, the dispersion equations were solved numerically for the fluid-filled cylindrical cavity in an elastic media allowing for the solution of the phase velocity, group velocity and the attenuation curves [18].

Considerable attenuation of the creeping Rayleigh wave through generation of halo (or whispering gallery) waves into the fluid-filled cylinder was found to greatly hinder the performance of the inspection technique. A transient time domain solution for a shear plane wave was also solved in order to calculate the precise attenuation of the circumferential wave, separate from the re-radiated halo wave [20]. From these solutions, it was clearly demonstrated that the 'leaky' Rayleigh wave that propagates about a fluid-filled cylindrical hole with no crack would be difficult to detect due to excessive loss into the fluid.

In order to develop a robust ultrasonic inspection methodology for a fluid-filled cylindrical hole, additional modeling insight is required. No prior work was found which investigated the scattering of an incident shear transducer signal for the case of a fluid-filled cavity with a radial crack or notch. To best model these configurations, boundary element method (BEM) models of the ultrasonic scattering process are developed in this Dissertation. Some prior studies have investigated the scattering of a fluid-filled cavity in an elastic medium using the boundary element method. Niwa et al examined the transient scattering of a plane elastic wave by a fluid-filled inclusion in an elastic half space using the frequency domain boundary integral equation method [25]. Their work will be the basis for the development of BEM models of a fluid-filled cavity with a fluid-filled notch. With these models, parametric studies of the pulse-echo and pitch-catch responses will be performed to determine the most robust methodology to detect the existence of a top notch.

5.2 BEM Model Development

Figure 5.1 displays the configurations of a fluid-filled cylindrical hole for the no-notch (a) and notch (b) cases. The notch is finite in width and filled with a fluid. To minimize computational time, a single boundary is used to define the shape of the cylindrical hole and the notch. The frequency domain BEM formulation presented here is based on the derivation for a fluid inclusion presented by Niwa et al [25].

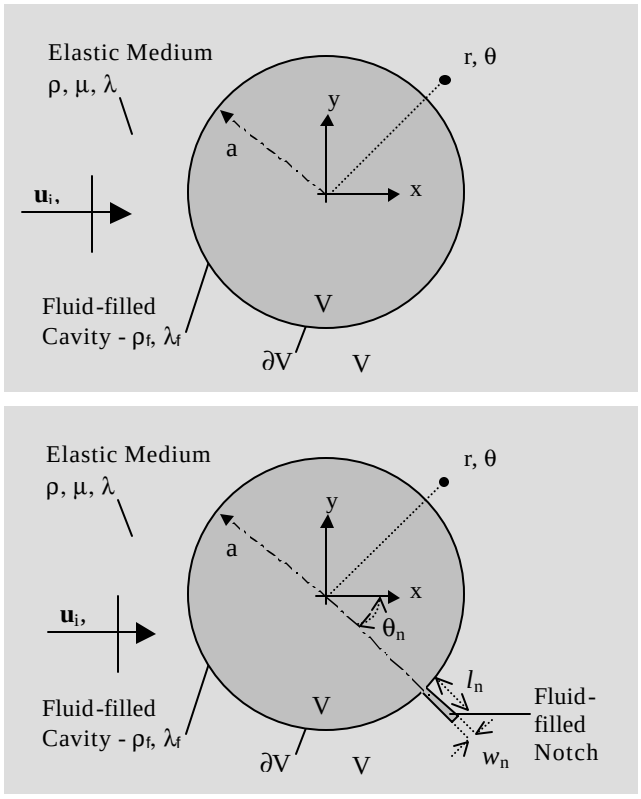

Figure 5.1. Fluid-filled cylindrical cavity in an infinite elastic medium for (a) no-notch case and (b) with-notch case.

The equation of motion for an elastic solid is given by

$$(\lambda + \mu)\tilde{\nabla}\tilde{\nabla} \cdot \mathbf{u}(\mathbf{x},t) + \mu\nabla^2\mathbf{u}(\mathbf{x},t) = \rho\,\ddot{\mathbf{u}}(\mathbf{x},t)\,. \tag{5.1}$$

To define the traction conditions, Hooke's law and the expression for the strains are used. The equation of motion for an inviscid fluid is given by

$$\lambda_f \nabla^2 p(\mathbf{x},t) = \rho_f\,\ddot{p}(\mathbf{x},t)\,, \tag{5.2}$$

where $p(\mathbf{x},t)$ is the fluid pressure. A linear inviscid constitutive relation can be derived as

$$-\tilde{\nabla} p(\mathbf{x},t) = \rho_f \ddot{\mathbf{u}}(\mathbf{x},t)\,. \tag{5.3}$$

The steady state form of the equation of motion in the transformed domain for an elastic solid follows from Eq. (5.1) as

$$(\lambda + \mu)\tilde{\nabla}\tilde{\nabla} \cdot \hat{\mathbf{u}}(\mathbf{x},\omega) + \mu\nabla^2\hat{\mathbf{u}}(\mathbf{x},\omega) + \rho\omega^2\hat{\mathbf{u}}(\mathbf{x},\omega) = 0\,, \tag{5.4}$$

The steady state form of the equation of motion for an inviscid fluid is given by

$$\lambda_f \nabla^2 \hat{p}(\mathbf{x},\omega) + \rho_f \omega^2 \hat{p}(\mathbf{x},\omega) = 0\,, \tag{5.5}$$

where the constitutive relation (5.3) becomes

$$\tilde{\nabla}\hat{p}(\mathbf{x},\omega) = \rho_f \omega^2 \hat{\mathbf{u}}(\mathbf{x},\omega)\,. \tag{5.6}$$

Of particular interest is the relationship at the boundary of the fluid where,

$$\hat{u}_n(\mathbf{x},\omega) = \frac{1}{\rho_f \omega^2}\frac{\partial \hat{p}(\mathbf{x},\omega)}{\partial n}\,. \tag{5.7}$$

The interface conditions for an inviscid fluid-filled cylindrical cavity in an elastic medium are continuity of displacement between the elastic solid and the fluid

$$\mathbf{n} \cdot \hat{\mathbf{u}}(\mathbf{x},\omega)\Big|_{r=a} = \frac{1}{\rho_f \omega^2}\frac{\partial \hat{p}(\mathbf{x},\omega)}{\partial n}\Bigg|_{r=a}\,, \tag{5.8}$$

and continuity of normal traction where

$$\hat{t}_n(\mathbf{x},\omega)\Big|_{\mathrm{r=a}} = -\hat{p}(\mathbf{x},\omega)\Big|_{r=a}, \tag{5.9}$$

while the shear traction for the elastic medium is equal to zero on r = a

$$\hat{t}_t(\mathbf{x},\omega)\Big|_{\mathrm{r=a}} = 0, \tag{5.10}$$

Consider an incident displacement field in the elastic medium, $\mathbf{u^i}$. The field scattered from the interface between the fluid cavity and the elastic solid will be defined as $\mathbf{u^{sc}}$. Thus the superposition of these two fields gives the total field response in the elastic medium, $\mathbf{u^t}$. The scattered response in the fluid-filled cylinder will be defined in terms of pressure, p^f. By substituting the displacements, $\mathbf{u^i} + \mathbf{u^{sc}}$, for $\mathbf{u^t}$, and the tractions, $\mathbf{t^i} + \mathbf{t^{sc}}$ for $\mathbf{t^t}$, and applying the relation (5.7) , the interface conditions become,

$$\mathbf{n}\cdot\hat{\mathbf{u}}^{sc}(\mathbf{x},\omega) - \frac{1}{\rho_f \omega^2}\frac{\partial \hat{p}^f}{\partial n}(\mathbf{x},\omega) = -\mathbf{n}\cdot\hat{\mathbf{u}}^{i}(\mathbf{x},\omega), \quad \mathrm{r = a}, \tag{5.11}$$

$$\hat{t}_n^{sc}(\mathbf{x},\omega) + \hat{p}^f(\mathbf{x},\omega) = -\hat{t}_n^{i}(\mathbf{x},\omega), \quad \mathrm{r = a}, \tag{5.12}$$

$$\hat{t}_t^{sc}(\mathbf{x},\omega) = -\hat{t}_t^{i}(\mathbf{x},\omega), \quad \mathrm{r = a}. \tag{5.13}$$

Integral representations for both the elastic medium and the fluid-filled cavity can now be defined through a reciprocity relation for two dynamic states. By applying the interface conditions and evaluating the limit as a point load state approaches the interface, an integral equation for an infinite elastic domain can be written as

$$\int_{\partial V}\left[\mathbf{U}(\mathbf{x},y;\omega)\hat{\mathbf{t}}^{sc}(y,\omega) - \mathbf{T}(\mathbf{x},y;\omega)\hat{\mathbf{u}}^{sc}(y,\omega)\right]\mathrm{dS_y} = \begin{matrix}\hat{\mathbf{u}}^{sc}(\mathbf{x};\omega), & \mathbf{x}\in \mathrm{V} \\ 0, & \mathbf{x}\in \mathrm{V}^f\end{matrix}. \tag{5.14}$$

Likewise, an integral equation for the fluid-filled cylinder can be represented by

$$\int_{\partial V}\left[\frac{\partial P}{\partial n}(\mathbf{x},y;\boldsymbol{w})\,\hat{p}^{f}(y,\boldsymbol{w})-P(\mathbf{x},y;\boldsymbol{w})\frac{\partial \hat{p}^{f}}{\partial n}(y,\boldsymbol{w})\right]\mathrm{dS}_{y}=-c\hat{p}^{f}(\mathbf{x};\boldsymbol{w}),\quad \mathbf{x}\in \mathrm{V}^{f}\,. \tag{5.15}$$

For the infinite elastic domain, the fundamental solution for the two dimensional problem, **U,** the double layer kernal, **T,** are given respectively by

$$\mathbf{U}(\mathbf{x},y)=\frac{i}{4m}\left[H_0^{(1)}(k_T r)+\frac{1}{(k_T)^2}\nabla\nabla\left(H_0^{(1)}(k_T r)-H_0^{(1)}(k_L r)\right)\right], \tag{5.16}$$

$$\mathbf{T}(\mathbf{x},y)=\overset{n}{\mathbf{T}}(l,m,\partial_y)\mathbf{U}(\mathbf{x},y)\,. \tag{5.17}$$

For the fluid domain, the fundamental solution for the two dimensional problem, *P*, is given by

$$P(\mathbf{x},y)=\frac{i}{4}H_0^{(1)}(k_f r). \tag{5.18}$$

Equations (5.16-5.18) can be found in the paper by Niwa et al [25].

In the next step, the boundaries are discretized into elements, and two separate systems of equations are derived for the integral equations. The details by which these matrix equations are derived can be found in the literature [26-28]. The result can be represented by the following matrix equations for the elastic solid and fluid-filled cavity respectively,

$$\mathbf{H}^{(1)}\hat{\mathbf{u}}^{sc}=\mathbf{G}^{(1)}\hat{\mathbf{t}}^{sc}, \tag{5.19}$$

$$\mathbf{H}^{(2)}\hat{p}^{f}=\mathbf{G}^{(2)}\frac{\partial \hat{p}^{f}}{\partial n}, \tag{5.20}$$

With the application of the boundary conditions (5.11-5.13) to these equations (5.19-5.20), a single system of equations can be written in the form

$$\begin{bmatrix} \mathbf{H}^{(1a)} & -\mathbf{G}^{(1a)} \\ \mathbf{H}^{(1b)} & -\mathbf{G}^{(1b)} \\ \rho_f \omega^2 \mathbf{G}^{(2')} & \mathbf{H}^{(2')} \\ 0 & \mathbf{A}^{(2)} \end{bmatrix} \begin{Bmatrix} \hat{\mathbf{u}}^{sc} \\ \hat{\mathbf{t}}^{sc} \end{Bmatrix} = \begin{pmatrix} 0 \\ 0 \\ \mathbf{B}^{(1)} \\ \mathbf{B}^{(2)} \end{pmatrix}, \tag{5.21}$$

By solving this matrix equation and applying the interface conditions (5.11-5.12) to the solution, the unknowns, $\hat{\mathbf{u}}^{sc}$, $\hat{\mathbf{t}}^{sc}$, $\hat{p}^{f}$, $\frac{\partial \hat{p}^{f}}{\partial \mathrm{n}}$, can be evaluated. A similar approach as discussed in prior work is implemented to solve for the total transient response [26].

5.3 Validation of BEM Simulation with an Analytic Model

The analytic solution for the displacement and tractions around a fluid-filled cavity in an infinite elastic domain for plane harmonic shear waves has been derived [49,51,52]. This solution was used to validate the boundary element method solution for the no-notch case. Comparisons between the 'exact' and the BEM solutions were made for the displacement in the y-direction normalized with respect to the magnitude of the incident plane wave. Figures 5.2 and 5.3 plot these displacements at locations on the hole interface for θ from 0 to 180 degrees for different plane wave frequencies ($k_T a = 3.983$ and $k_T a = 7.966$ respectively). Excellent agreement was found between the exact and BEM solutions.

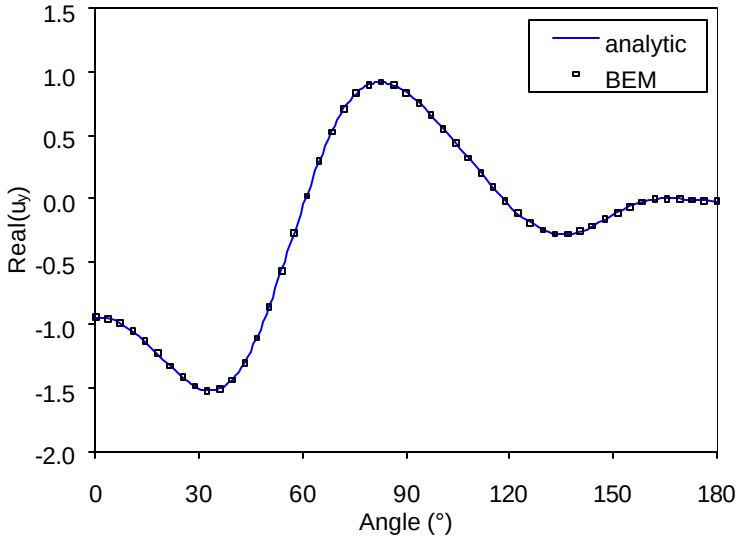

Figure 5.2. Comparison of analytic and BEM solutions for response to plane harmonic shear wave – $k_T a = 3.983$.

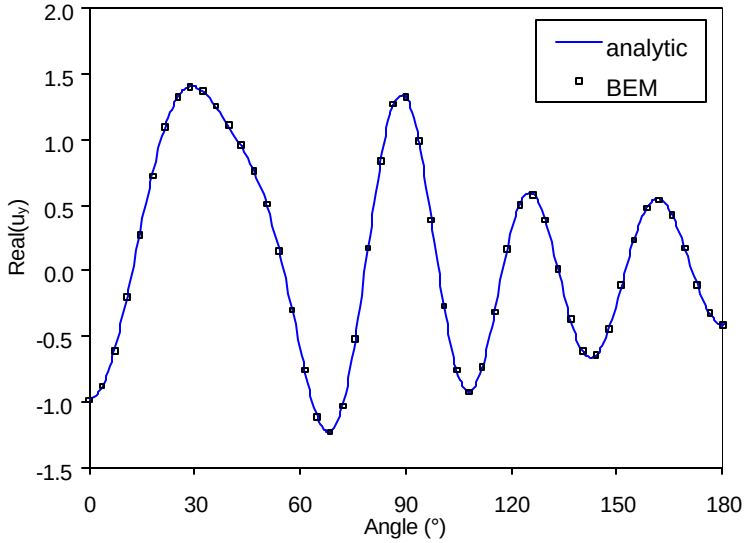

Figure 5.3. Comparison of analytic and BEM solutions for response to plane harmonic shear wave – $k_T a = 7.966$.

5.4 Discussion of BEM Simulation and Experimental Results

Figures 5.4 and 5.5 display contour plots of the total field response to an incident in-plane shear pulse on a fluid-filled cylindrical cavity for no-notch and with-notch cases respectively, for nine subsequent times. The magnitude of the in-plane displacement for each field location is represented by a gray scale, where the darkest and lightest regions represent locations of greatest and lowest amplitude, respectively. The plots represent nine snapshots in time where $\tau = 0,1,2,3,4,5,6,7,8$ and τ is defined by $\tau = (t-t_o)*c_t/a$ (c_t is the shear wave speed of the material, a is the radius of the weep hole and t_o is a reference time.) The properties of water were used for the fluid. The transducer and elastic parameters for the simulation are presented in Appendix A.

Insight can be gained from the scattering response for the no-notch case. Initial reflection of longitudinal and transverse waves of the incident transverse wave is first observed. In addition, a longitudinal wave is transmitted into the fluid-filled cavity. The incident transverse wave also generates a Rayleigh wave that propagates along the surface of the weep hole. As for the empty cavity case, the Rayleigh wave can clearly be observed leaking energy into the surrounding solid due to the curvature of the weep hole and thus generating a significant circumferential shear wave that propagates from the hole. However, a significant loss of the 'leaky' Rayleigh wave in the form of a longitudinal wave into the fluid at the Rayleigh angle is also observed. The term, halo wave, has been used for this wave in the fluid [18-21]. This loss into the fluid causes the

'leaky' Rayleigh wave to die out much faster than for the no-fluid case. As time marches forward, a halo wave continues to propagate through the fluid, becomes incident upon the wall of the cavity, and transmits a portion of the wave back into the elastic media. Thus the reradiated waves from the fluid dominate the signal which returns to receiving transducer. This series of contour plots clearly displays the phenomenon of the 'doubly leaky' Rayleigh wave initially described by Hassan and Nagy [18-21].

Observations can also be made from the scattering response for the notch case. Again, the initial reflection of longitudinal and transverse signals and the longitudinal wave transmission into the fluid by the incident transverse wave are first observed. The incident transverse wave again generates a Rayleigh wave that propagates along the surface of the weep hole. With a top notch present, a portion of the 'leaky' Rayleigh wave is reflected. The reflected Rayleigh wave leaks energy into the riser and thus generates a small but detectable circumferential shear wave that propagates from the hole. Time step τ=4 displays this detectable signal. As for the empty cylindrical hole case, the pitch transducer can be used to detect this signal. These observations indicate a possible method for detecting the existence of a top notch on a fluid-filled weep hole.

Additional observations can be made for the notch case. Again, a significant loss of the propagating 'leaky' Rayleigh wave into the fluid as a halo wave is observed. However, the magnitude of the halo wave transmitted into the fluid for the notch case is not as great as for the no-notch case. Since a portion of the 'leaky' Rayleigh wave is reflected before the signal is leaked into the fluid, the transmitted halo wave in the fluid is reduced. This results in the first reradiated halo wave being significantly smaller for the

notch case. Time step τ=8 clearly displays this reduction in the magnitude of the first reradiated halo wave. As for the empty cylindrical hole case, a second transducer located above the pitch transducer can be used to detect this signal. These observations indicate another possible method for detecting the existence of a top notch.

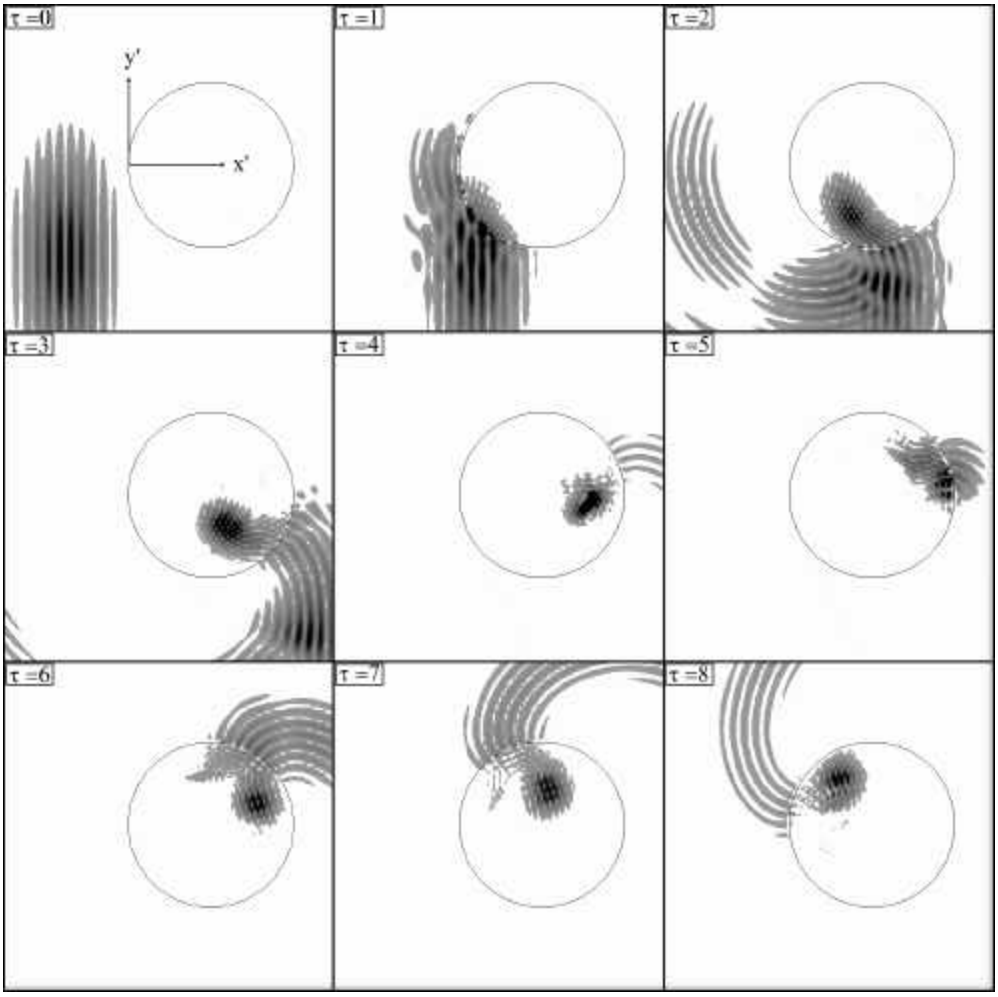

Figure 5.4. Contour plots of the total displacement field response to an incident in-plane shear pulse on a 1/4" fluid filled weep hole with no crack for nine time steps, τ = 0,1,2,3,4,5,6,7,8.

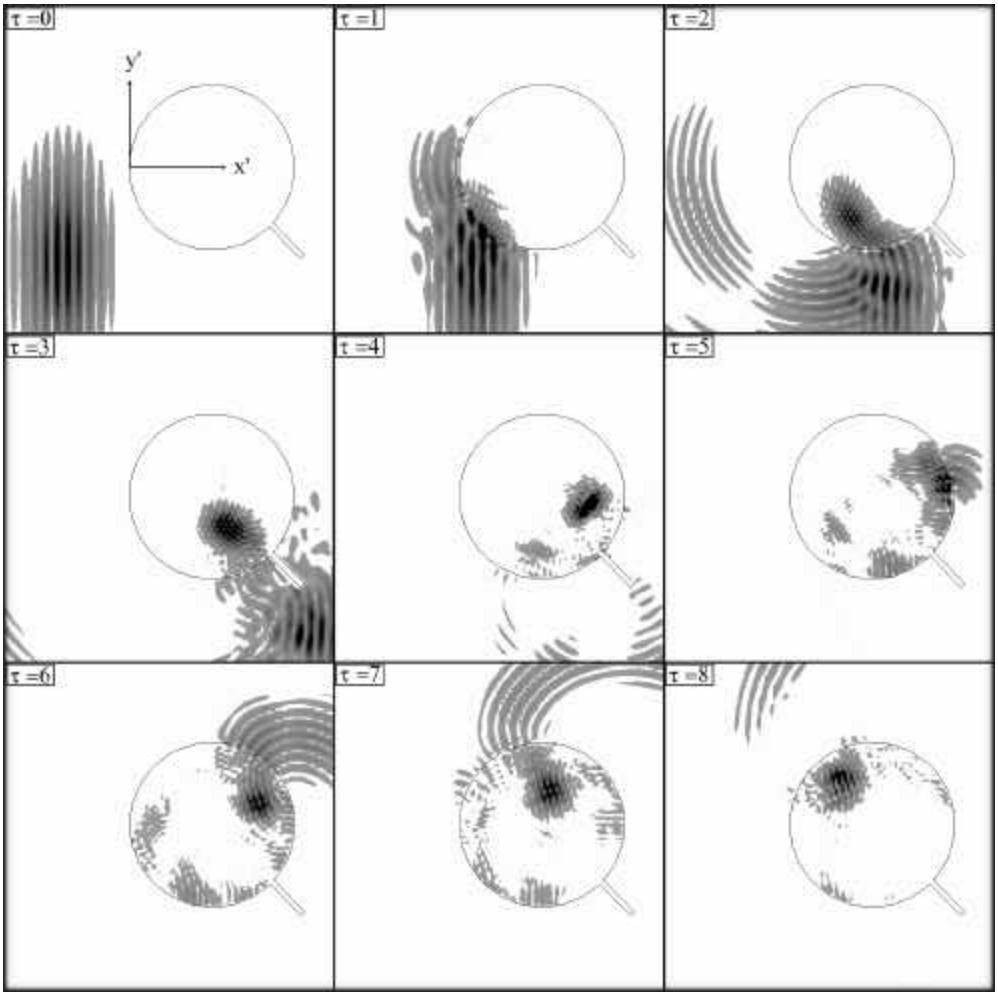

Figure 5.5. Contour plots of the total displacement field response to an incident in-plane shear pulse on a 1/4" fluid filled weep hole with a 0.063" notch for nine time steps, τ = 0,1,2,3,4,5,6,7,8.

A comparison of the transducer response for the BEM simulation with experimental results was made. Figures 5.6 and 5.7 display the comparison of pulse-echo and pitch catch signals respectively for four cases: (a) no notch, no fluid in weep hole, (b)

no notch, with fluid in weep hole, (c) with notch, no fluid in weep hole, and (d) with notch, with fluid in weep hole. The magnitude of the BEM simulations was adjusted to match the average specular refection for the experimental data set. Details concerning the simulation parameters are given in Appendix A. Overall, there is good agreement between the simulated and experimental data.

For the pulse-echo response, the notch case is shown to generate a significant reflected 'leaky' Rayleigh wave signal for both the empty and the fluid-filled hole cases. Although the magnitude of the reflected 'leaky' Rayleigh wave signal for the fluid-filled hole case (d) is about 30% of the magnitude for the empty hole case (c), this signal is still significantly greater than the noise level for the no-notch case (b). It can be observed that accurate placement of gating can improve the signal to noise ratio significantly.

For the pitch-catch response data, several observations can be made. First, as discussed by Hassan and Nagy, the transmitted circumferential Rayleigh wave is reduce considerably by the addition of fluid to the insert. In addition, two significant reradiated halo waves are also shown for the fluid filled cases. As observed in the contour plots, there is a significant reduction in the magnitude of the first reradiated halo wave due to the existence of a top notch. Simulated results produce a reduction of about 50% for larger notch cases. A reduction that varies between 20% to 60% for larger notch cases has been observed experimentally. These discrepancies may be caused by variation in experimental top-notch locations ($\theta_n = 45°$ for the BEM simulation), differences in locating the transducers, transducer model approximations and experimental noise. One significant challenge toward implementing this approach is the requirement for accurate

gating of the first reradiated halo wave signal, due to its close proximity to the second reradiated halo wave signal in the time domain. An interesting observation concerning the second reradiated halo wave is that there is little difference in magnitude for the notch and no-notch cases. Since the primary source of the second reradiated halo wave is due to the initial bulk transmission into the fluid, a signal from a top notch will not interfere with the propagation of this part of the signal. Since both the first and second reradiated halo waves are significant in magnitude for a wide range of notch sizes, their location can be determine using a straightforward search algorithm. Following the location of both peaks, a gate can easily be located about the first peak to determine the magnitude of the first reradiated halo wave.

BEM simulation studies were performed to evaluate the sensitivity of the scattering response sensitivity to changes in notch length. Figure 5.8 display the peak to peak response for the BEM simulation of the reflected 'leaky' Rayleigh wave signal (acquired in the pulse-echo mode) and the first reradiated halo wave signal (acquired in the pitch-catch mode) for various notch lengths. This data indicates a sensitivity to changes of 0.010 in. in a range of top notch detectability for both the reflected 'leaky' Rayleigh wave signal and the initial reradiated halo wave signal. Clearly, both of these signals can be used for detection of relatively small top notches for fluid-filled cases. The sensitivity of top-notch detection for the fluid-filled hole case is comparable to prior results for the empty hole case [16,22,23].

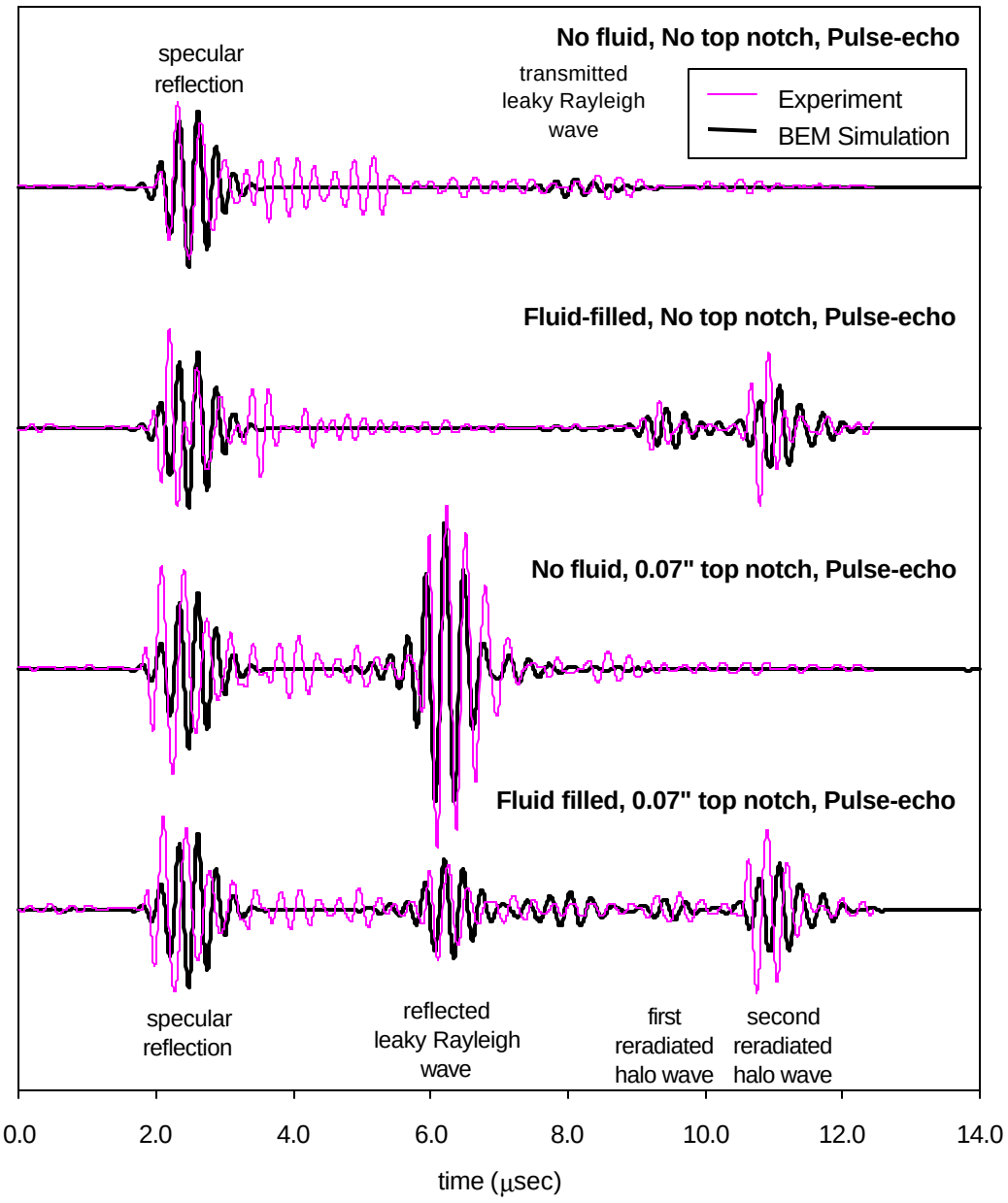

Figure 5.6. Pulse echo signals comparing BEM simulations and experimental data for four cases: (a) no notch, no fluid in weep hole, (b) no notch, with fluid in weep hole, (c) with notch, no fluid in weep hole, (d) with notch, with fluid in weep hole.

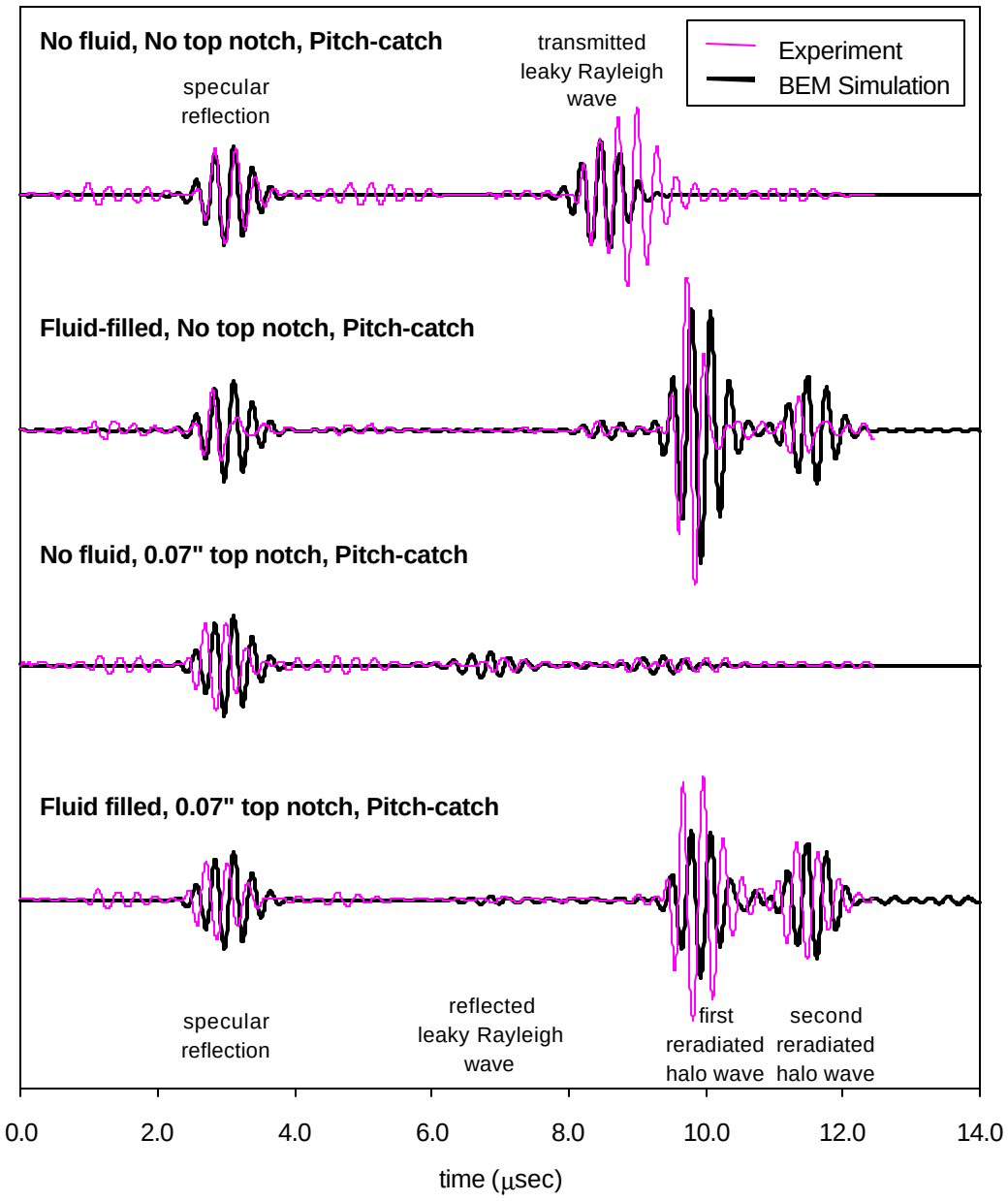

Figure 5.7. Pitch catch signals comparing BEM simulations and experimental data for four cases: (a) no notch, no fluid in weep hole, (b) no notch, with fluid in weep hole, (c) with notch, no fluid in weep hole, (d) with notch, with fluid in weep hole.

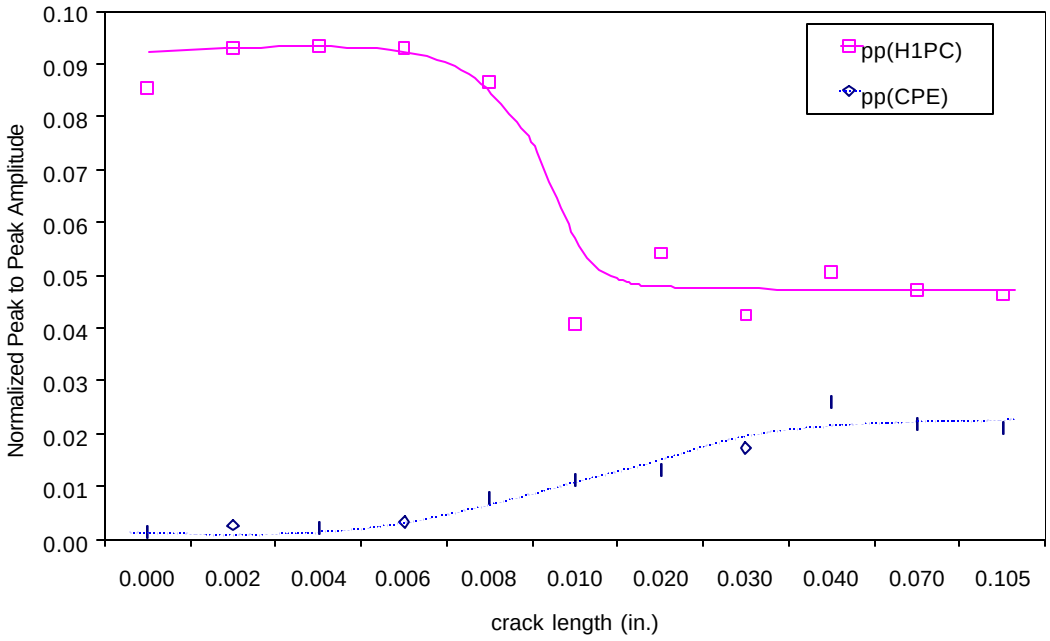

Figure 5.8. Amplitude plot for the BEM simulation of reflected 'leaky' Rayleigh wave signals (CPE$^{\diamond}$) and reradiated initial halo wave signals (H1PC$^{\square}$) for various notch sizes.

5.5 Methodology for Top Crack Detection for a Fluid-Filled Cylindrical Hole

Five measurement strategies were investigated for optimal top crack detection for fluid filled holes:

- M1 = Measure of peak to peak amplitudes of the reflected 'leaky' Rayleigh wave by the pitch transducer,
- M2 = Measure of peak to peak amplitudes of the first reradiated halo wave by the pitch transducer,
- M3 = Measure of peak to peak amplitudes of the first reradiated halo wave by the catch transducer,
- M4 = Measure of ratio of the reflected 'leaky' Rayleigh wave received by pitch transducer to the first reradiated halo wave received by pitch transducer (as reference signal) : M1/M2,
- M5 = Measure of ratio of the amplitudes of the reflected 'leaky' Rayleigh wave by pitch transducer to the first reradiated halo wave by catch transducer (as reference signal) : M1/M3.

The measures, M1, M2, and M4, would be advantageous since they would only require a single transducer to perform the inspection. The measures, M4 and M5, are ratios that essentially use the first reradiated halo wave as a reference signal. These measures should be more robust to experimental variation in transducer coupling.

All of these measures were found to properly classify all notches larger than 0.010 in. for a simulated data set. Figure 5.9 displays the measure M5 for various numerically simulated notch length cases. Clearly, notches 0.010 in. and larger can be properly classified using this ratio approach.

Seven no-notch and seven notch weep hole samples were investigated experimentally. The sawcut notch lengths varied between 0.055 and 0.075 in. Gates were used to measure the peak-to-peak signals from the reflected 'leaky' Rayleigh wave and the first reradiated halo wave. The results are presented in Table 5.1. For all five measures, proper classification of all no-notch and notch cases was made.

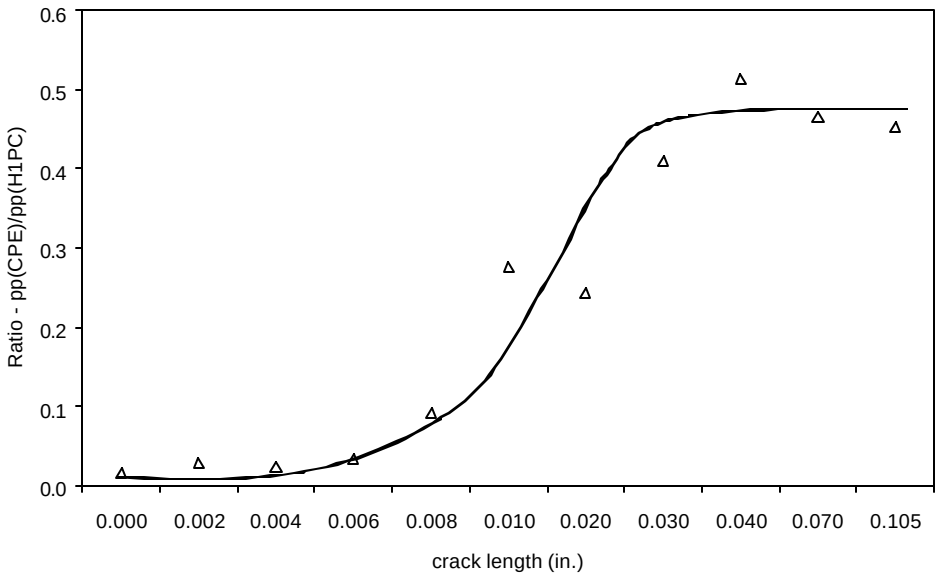

Figure 5.9. Plot from BEM simulation of M5, the amplitude ratio of the reflected 'leaky' Rayleigh wave signal (acquired in pulse-echo mode) and the reradiated initial halo wave signal (acquired in pitch-catch mode), for various notch sizes.

In order to determine which of these measures is the best statistically, given this limited data set, several analysis approaches were investigated. To determine the probability of a missed classification (missed crack or false call) for a particular measure, general statistical analysis approaches require the assumption of normal distributions. The Anderson - Darling test can be used to determine the degree of normality for a data set [53,54]. Table 5.2 displays an assessment of normality of the no-notch and notch data sets for each of the measures. All but one of the data sets satisfy the criteria for a normal distribution. The single case which does not (M3 - no notch case), is due to saturation of the measurement voltage resulting in a limit value of 255 for the 8 bit A/D converter. This one case should not distort the statistical analysis results. Table 5.3 displays the results for the probability of a correct classification for the finite data sets. Measures M1, M4 and M5 all exceeded the desired 95 percent correct classification with M5 and M4 exceeding 99 percent.

An alternative approach incorporates a Box Cox transformation of the data in order to optimize the measures for the greatest degree of normality [54,55]. The Box Cox transformation is essentially a power transformation of the form Y^{λ}. Each of the measures were optimized for the parameter λ for minimizing the degree of non-normality; the results are given in Table 5.4. Table 5.4 also displays the results for the probability of a correct classification of the Box Cox transformed data sets. Measure M5, the ratio of the reflected 'leaky' Rayleigh wave by pitch transducer to the first reradiated

halo wave by catch transducer, was found to be the best approach for correct classification again exceeding 99 percent.

Table 5.1. Experimental results for five measure approaches.

		M1 (reflected 'leaky' surf. wave – in PE)	**M2** (reradiated halo wave – in PE)	**M3** (reradiated halo wave – in PC)	**M4** (M1/M2)	**M5** (M1/M3)
Notch	1	63	15	164	4.20	0.38
Notch	2	47	19	161	2.47	0.29
Notch	3	51	15	155	3.40	0.33
Notch	4	87	24	228	3.63	0.38
Notch	5	56	17	184	3.29	0.30
Notch	6	57	23	183	2.48	0.31
Notch	7	45	11	104	4.09	0.43
No notch	1	10	32	255	0.31	0.039
No notch	2	10	32	233	0.31	0.043
No notch	3	15	49	255	0.31	0.059
No notch	4	8	48	255	0.17	0.031
No notch	5	11	28	242	0.39	0.045
No notch	6	21	71	255	0.30	0.082
No notch	7	13	35	255	0.37	0.051
Notch	MEAN	**58**	**18**	**168**	**3.37**	**0.35**
Notch	STD	**14**	**5**	**37**	**0.69**	**0.05**
No notch	MEAN	**13**	**42**	**250**	**0.31**	**0.050**
No notch	STD	**4**	**15**	**9**	**0.07**	**0.017**

Table 5.2. Anderson – Darling test for normality.

	M1 (reflected 'leaky' surf. wave – in PE)	**M2** (reradiated halo wave – in PE)	**M3** (reradiated halo wave – in PC)	**M4** (M1/M2)	**M5** (M1/M3)
Notch	0.118	0.682	0.419	0.440	0.378
No notch	0.234	0.129	**0.001**	0.068	0.468

Table 5.3. Probability of correct classification for measure.

	M1 (reflected 'leaky' surf. wave – in PE)	**M2** (reradiated halo wave – in PE)	**M3** (reradiated halo wave – in PC)	**M4** (M1/M2)	**M5** (M1/M3)
Prob(correct classification)	**0.975**	**0.869**	**0.935**	**0.996**	**0.998**

Table 5.4. Probability of correct classification for measure with Box Cox transformation for normal distribution.

	M1 (reflected 'leaky' surf. wave – in PE)	**M2** (reradiated halo wave – in PE)	**M3** (reradiated halo wave – in PC)	**M4** (M1/M2)	**M5** (M1/M3)
λ	-2	-1.25	2	3	0.333
Prob(correct classification)	**0.931**	**0.887**	**0.951**	**0.942**	**0.998**

Several issues must be addressed before this procedure can be implemented. Variation in the diameter of weep holes in the C-141 aircraft must be addressed. Due to depot maintenance resizing of weep holes that may have occurred, hole diameters may vary between 0.250 in. and 0.390 in. The BEM model was used to investigate this issue. Two larger holes diameters, 5/16" and 3/8", were compared with the standard 1/4" diameter weep hole. Table 4.5 lists the significant parameter settings for the simulation. Additional details for the simulation are given in Appendix A.

Figure 5.10 shows the simulated pulse-echo signals for three weep holes diameters for the 0.070 in. notch case. Clearly, the reflected leaky Rayleigh wave signal is shifted due to the increase in the diameter of the weep hole. Unlike the empty weep hole case where broad gates can be used due to the absence of other significant signals, the fluid-filled case may require tighter gates. Tighter gates are also preferred for improving the signal-to-noise ratio.

Figures 5.11 and 5.12 show the simulated pitch-catch signals for three weep hole diameters for the no-notch case and the 0.070 in. notch case, respectively. The first and second reradiated halo waves are also shifted due to the increase in the diameter of the weep hole. Due to the close proximity of the first and second halo waves, proper placement of tight gates about the first reradiated halo wave is an absolute requirement for accurate peak-to-peak measurement. Since the range of diameters is known, a neural network may be trained to determine the hole diameter and thus the proper gate location. The best approach to assess the hole diameter is by examining the time of flight between the specular reference signal (in pulse-echo mode) and the first and second reradiated

halo wave signals (in pitch-catch mode.) Although sizing of the hole diameter may be feasible using the reflected 'leaky' Rayleigh wave signal, consistent classification cannot be guaranteed due to possible variation in the top crack location. A schematic diagram is given in Figure 5.13 for the complete proposed scheme for top crack detection in fluid- filled weep holes.

Table 5.5. BEM simulations of weep hole diameter variation for top notch detection.

Hole Diameter (in.)	Number of elements	Pitch Transducer Location* (in.)	Pitch Transducer Location - x' (in.)	Pitch Transducer Location - y' (in.)
0.250	100	-0.200	-0.862	-0.141
0.3125	126	-0.250	-0.898	-0.177
0.375	150	-0.300	-0.933	-0.212

* - location of pitch transducer along bottom surface of wing from the weep hole reference location.

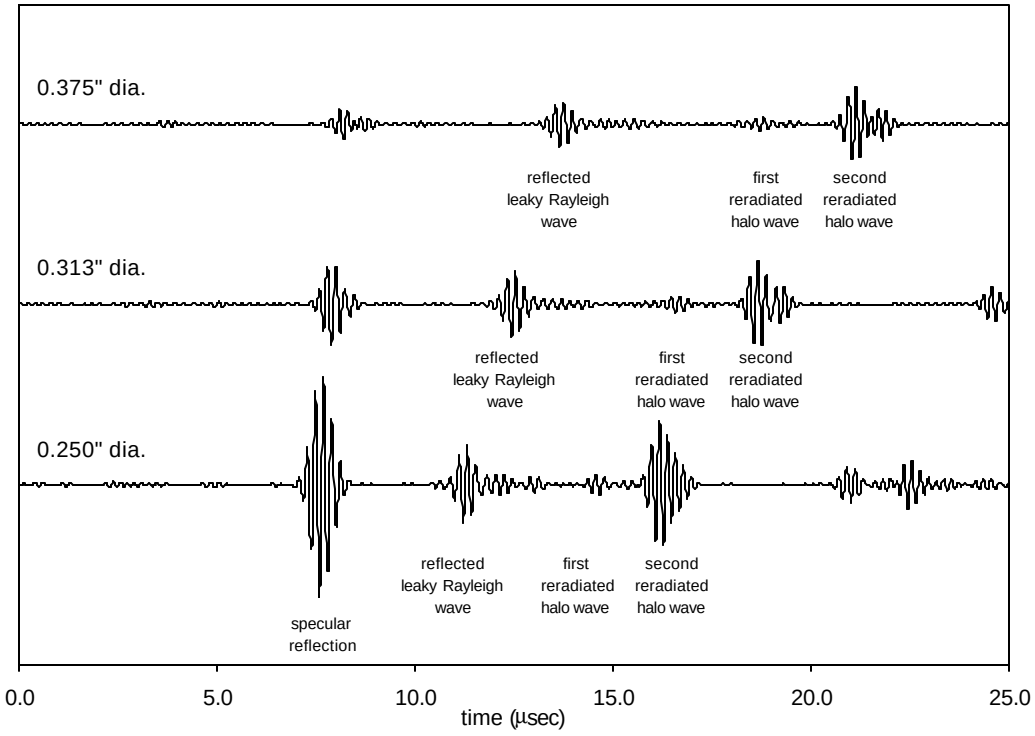

Figure 5.10. BEM pulse echo signals for various weep hole diameters (0.070" notch.)

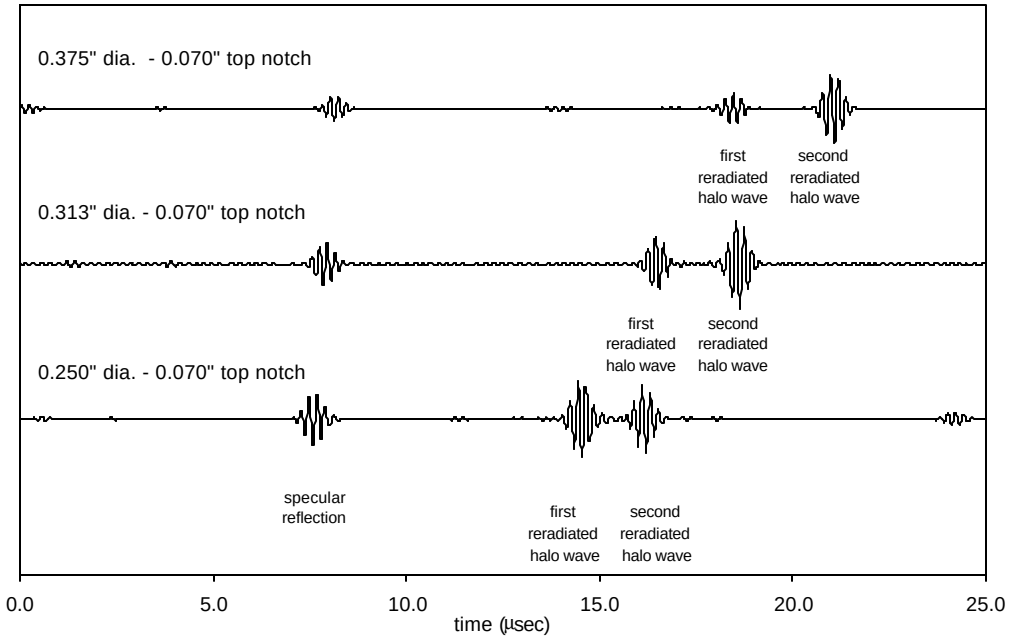

Figure 5.11. BEM pitch catch signals for various weep hole diameters (no notch case.)

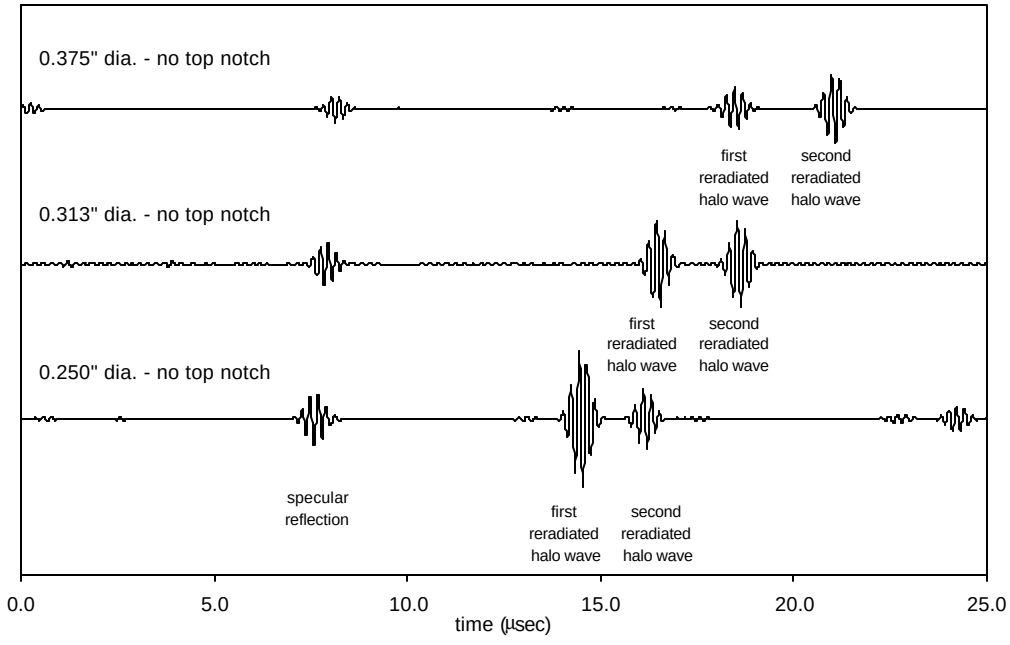

Figure 5.12. BEM pitch catch signals for various weep hole diameters (0.070” notch.)

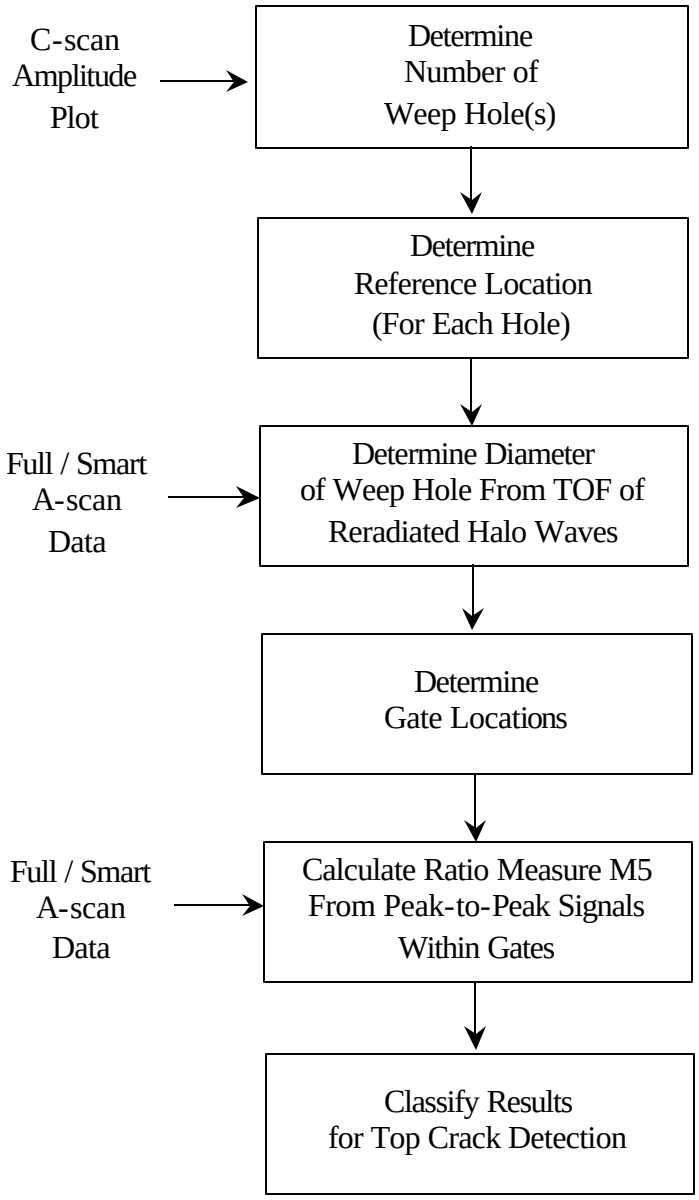

Figure 5.13. Schematic diagram of the proposed scheme for top-crack detection for fluid filled weep holes.